Electronic Supplementary Material (ESI) for Nanoscale.
This journal is © The Royal Society of Chemistry 2023

Supplementary Information

Lanthanide metal-organic network featuring a strong perpendicular magnetic anisotropy

Sofia O. Parreiras,*†[a] Daniel Moreno,†[a] Shanmugasibi K. Mathialagan,[a] Beatriz Muñiz-Cano,[a] Cristina Martín-Fuentes,[a] María Tenorio,[a] Lenka Černa,[b] José I. Urgel,[a] Koen Lauwaet,[a] Manuel Valvidares,[c] Miguel A. Valbuena,[a] José M. Gallego,[a,d] José I. Martínez,[d] Pierluigi Gargiani,[c] Rodolfo Miranda,[a,e] Julio Camarero,[a,e] and David Écija*[a]

[a.] *Instituto Madrileño de Estudios Avanzados en Nanociencia (IMDEA Nanoscience), Madrid 28049, Spain.*
[b.] *Brno University of Technology, 601 90, Czech Republic.*
[c.] *ALBA Synchrotron Light Source, Cerdanyola del Vallès 08290, Spain.*
[d.] *Instituto de Ciencia de Materiales de Madrid (ICMM-CSIC), Cantoblanco, Madrid 28049, Spain.*
[e.] *Departamento de Física de la Materia Condensada and Condensed Matter Physics Center (IFIMAC), Universidad Autónoma de Madrid, Madrid 28049, Spain.*

* Email: sofia.oliveira@imdea.org, david.ecija@imdea.org

Experimental methods

p-terphenyl-4,4′-dicarboxylic acid (TDA) molecules were purchased from BLDpharm. The molecules were deposited on a clean Cu(111) substrate, prepared by cycles of sputtering (Ar^+, 1.5 keV) and annealing (723 K, 10 min), by organic molecular beam epitaxy (OMBE) with a Kentax evaporator with the substrate heated to 373 K. Er atoms were deposited by e-beam evaporation from a metal rod (EFM3Ts evaporator) with the substrate still maintained at 373 K. The samples were post-annealed at 400 K. All the experiments were performed *in-situ* in UHV chambers with base pressures below $5x10^{-10}$ mbar. Scanning tunneling microscopy (STM) and spectroscopy (STS) experiments were carried out on an Omicron LT-STM at 4 K using tungsten tips. d*I*/d*V* spectra were measured with an open feedback loop and d*I*/d*V* maps with a closed feedback loop.

The synchrotron sample was prepared with an excess of molecules to ensure that all Er atoms were coordinated with molecules and there was no magnetic signal from Er clusters. Before the magnetic measurements the sample morphology and the absence of Er clusters were checked using a RHK Pan Flow STM operating at liquid nitrogen temperatures (LN_2) using tungsten tips.

X-ray absorption spectroscopy (XAS), X-ray linear dichroism (XLD) and X-ray magnetic circular dichroism (XMCD) experiments were performed at the BOREAS beamline of the ALBA synchrotron light source, Spain.[S1] The measurements were done in the total electron yield (TEY) mode, with a 90% circularly polarized beam and applying magnetic fields up to 6 T in the direction of the X-ray beam incidence. XLD is defined as the difference between XAS spectra measured with vertical and horizontal polarizations $(\mu_V - \mu_H)$. The spectra were measured at 0.05 T and 6 T and normalized at the maximum of Er M_5-edge of the isotropic spectra: $XNLD_{Iso} = (\frac{1}{3}\mu_V + \frac{2}{3}\mu_H)$. XMCD is determined by the difference between the circularly polarized XAS spectra taken with negative and positive polarizations $(\mu_- - \mu_+)$, and were normalized by the maximum of the Er M_5-edge of the average absorption spectra: $XAS_{Ave} = \left(\frac{\mu_+ + \mu_-}{2}\right)$.

The magnetization curves are constructed by evaluating the XMCD intensity of M_5-edge. The curves presented in figure 3c (main figure) were measured by a script that automatically changes the applied magnetic field and evaluate the signal at the maximum of M_5-edge and the pre-edge, which allows the calculation of the dichroic signal at different fields. In the case of the inset in figure 3c the curves were constructed by measuring XMCD spectra at some selected fields. This procedure reduces the number of points, but the resulting curves does not present the noise observed in the curves generated by the script.

Sum-rule analysis[S2,S3] was used to calculate the expectation values of the effective spin $\langle S_{zeff} \rangle = \langle S_z \rangle + 3\langle T_z \rangle$ and orbital $\langle L_Z \rangle$ magnetic moments (in units of $\hbar$). The spin moment $\langle S_z \rangle$ was determined assuming a theoretical value $\frac{\langle T_z \rangle}{\langle S_z \rangle} = +0.213$ for Er^{+3}.[S4] The relation $m_T = 2\langle S_z \rangle + \langle L_z \rangle$ was used to calculate the total magnetic moment per atom in μ_B. The moment anisotropy of m_T is defined as the difference between the projections of the magnetic moments at grazing and normal incidences in a field of 6 T and at a temperature of 1.7 K, $\Delta m_T = m_T(70°) - m_T(0°)$.

Stability at room temperature

STM measurements performed at room temperature (RT) confirmed the stability of the network at this temperature, as can be observed in Figure S1.

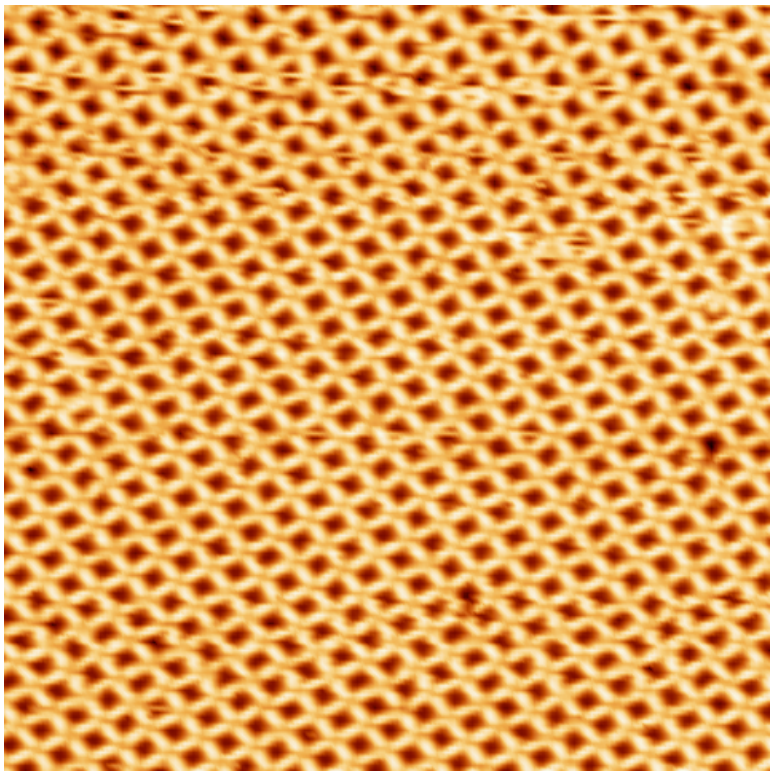

Figure S1. STM image of the Er-TDA network. Scanning parameters: V_b = 2.0 V and I_t = 50 pA, T = 300 K, image size: 17x17 nm^2.

UPS and ARPES results

An Er-TDA network has been measured by Ultraviolet Photoelectron Spectroscopy (UPS) and Angle-Resolved Photoemission Spectroscopy (ARPES). The sample was prepared in the same UVH chamber as the STM samples and transferred to the UPS/ARPES chamber in a UHV suitcase. The sample was measured at room temperature (RT), with a photon energy of $h\nu$ = 21.2 eV. STM measurements were performed at RT before the transference to ensure the stability of the system at this temperature (see Fig. S1 in the previous section). The UPS/ARPES measurements are presented in Fig. S2. All displayed spectra have been measured along the ΓK direction of the Cu(111) Surface Brillouin Zone parallel to the entrance slit of the analyser.

In panel S2a both overall UPS spectra from a clean Cu(111) surface and the Er-TDA network grown on Cu(111), spanning the whole valence band (VB) of Cu(111) are presented. By comparing the spectra, several additional states can be observed in the Er-TDA network in the energy region from 7 to 12 eV, a multipeak structure that is associated to Er 4f states. A decrease in the intensity of the Cu(111) 3d VB states is also evident, as a consequence of the presence of the network. In the region closer to the Fermi level (FL) an energy shift downwards at the bottom of the Cu surface state (SS) is also observed. This energy shift, ΔE, towards the FL is better displayed in the ARPES maps in panels S2b and S2c and their corresponding Energy Distribution Curves (EDCs) in panels S2d and S2e.

The energy minimum of the parabola, E_0, of the surface state is E_0 = (244 ± 4) meV for the Er-TDA sample, while for pristine Cu(111) is E_0 = (357) ± 4 meV, resulting in an energy shift, $\Delta E \sim 110$ meV. The wave vector at FL, k_F, is preserved after the molecular network formation, which indicates that it is not a mere effect of doping or charge transfer, but rather that it is coupled to an increment of the effective mass: from $m^*_{SS\ Cu(111)}$ = (0.54 ± 0.09) m_{e^-} to $m^*_{SS\ Er\text{-}TDA}$ = (0.75 ± 0.01) m_{e^-}. Both effects have been previously described in similar metal-organic networks on noble metal surfaces and have been related to a partial confinement of the SS because of the supramolecular array.[S5-S7]

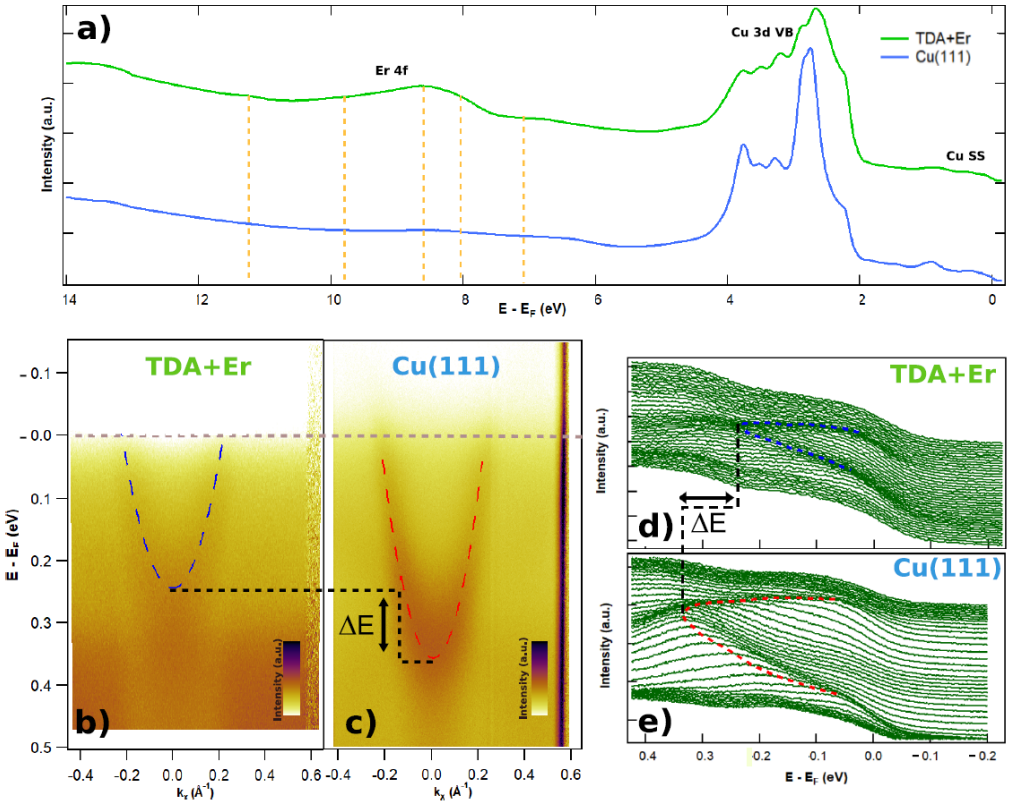

Figure S2. (a) UPS spectra for Er-TDA/Cu(111) and Cu(111). (b) and (c) SS ARPES band map for Er-TDA/Cu(111) and Cu(111), respectively. (d) and (e) EDCs extracted from spectra in panels (b) and (c).

Additional STS results

Short range STS measured close to Fermi are also indicative of a confinement of the surface state. As can be observed in Figure S3, there is a strong peak in the network pore (blue curve) around -0.18 V, shifted in energy when compared to the surface state of the Au(111) reference spectrum (green curve). STS spectra of the molecule and metallic centers (red and black curves, respectively) also present peaks at the same energy but featuring a much lower intensity. This peak is associated to the first resonance of the confined state. A peak resonance is observed around +0.14 V and is associated to the higher order resonance of the confined state. These results are similar to the observed in other porous metal-organic networks.[S8-S10]

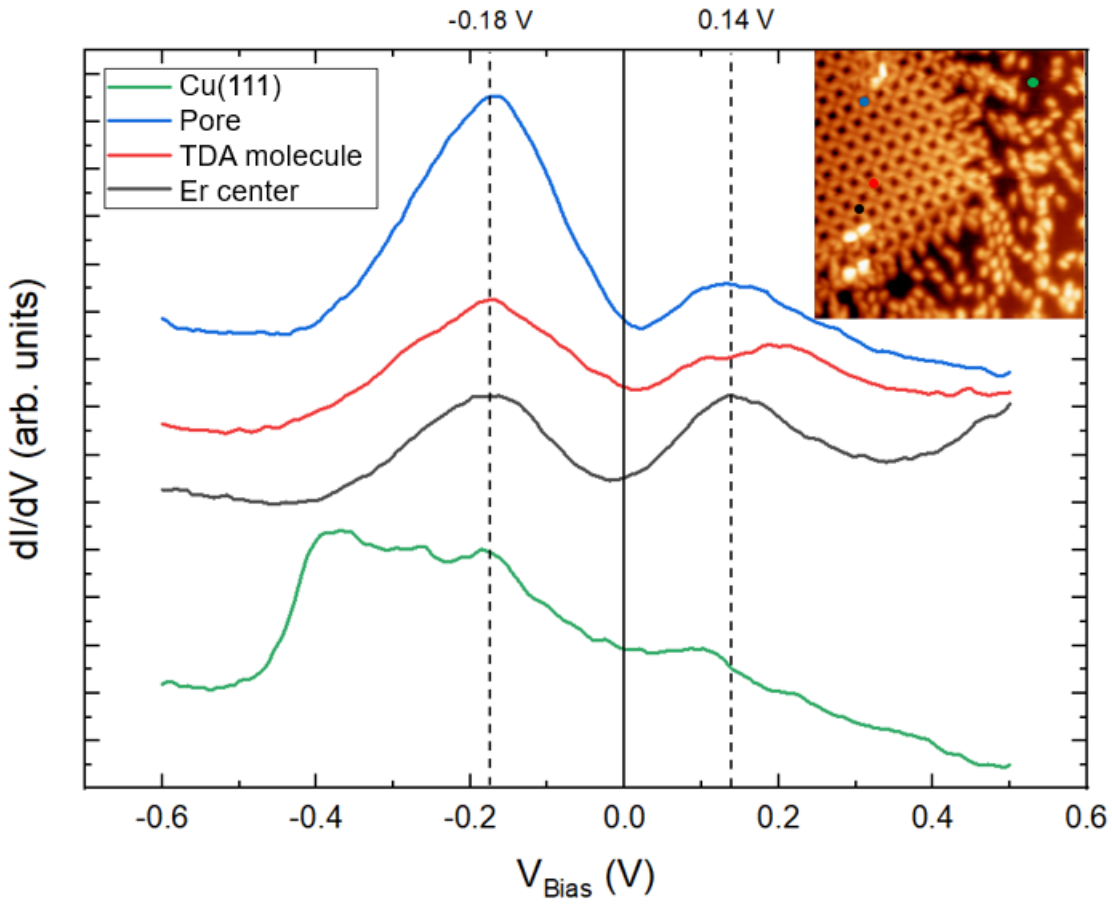

Figure S3. STS spectra taken at network pore (blue), TDA molecule (red), Er center (black), and Cu substrate (green). The dashed lines indicated the energies of the resonance peaks. The inset presents a reference STM image indicating the positions were the STS where taken. Scanning parameters: V_b = 500 mV and I_t = 20 pA, T = 4 K, image size: 30x30 nm^2. STS parameters: tip stabilization at V_b = 500 mV and I_t = 1.0 nA; lock-in modulation of 20 mV.

Theoretical Framework

All ab initio calculations have been performed by Density Functional Theory (DFT) as implemented in the plane-wave QUANTUM ESPRESSO simulation package.[S11] One-electron wave-functions were expanded in a plane-waves basis with energy cutoffs of 500 and 600 eV for the kinetic energy and the electronic density, respectively. For accounting for the exchange and correlation effects we have adopted the revised generalized gradient corrected approximation PBESol, [S12,S13] as well as for the Kresse-Joubert projector-augmented-wave pseudopotentials[S14] to model the ion–electron interaction for all the involved atoms (H, C, O, Cu, and Er) in order to include the spin-orbit coupling effect and a potential non-collinearity of spins. 22 valence electrons have been considered for the Er atom in order to check the role of the lanthanide $4f^{12}$ electrons in the subtle interfacial chemistry. Brillouin zone has been sampled by using optimal Monkhorst–Pack grids:[S15] (2×2×1) for structural optimizations and (4×4×1) for the computation of the electronic properties. To include dispersive forces within conventional density functionals we have adopted a perturbative van der Waals (vdW) empirical R^{-6} correction (DFT+D3).[S16] Atomic relaxations, carried out by using a conjugate gradient minimization scheme, were performed until the maximum force acting on any atom was below 0.02 eV $Å^{-1}$. The Fermi level was smeared within the Methfessel–Paxton parametrization[S17] with a Gaussian width of 0.01 eV, and all energies were extrapolated to T=0 K. Self-consistency in the electron density was converged to a precision in the total energy better than 10^{-6} eV.

Additional DFT results

In figure S4 is shown a simulated STM image together with an experimental one taken at the same tunneling current and bias voltage.

Figure S5 presents the calculated projected density of states (PDOS) onto the TDA molecule for the Er-TDA network on Cu(111). The PDOS is similar to the one calculated for Dy-TDA network on Cu(111)[S19] and also presents the LUMO resonance shifted to higher energies when compared to non-coordinated TDA molecules (see Fig. 2d of ref. [S19]).

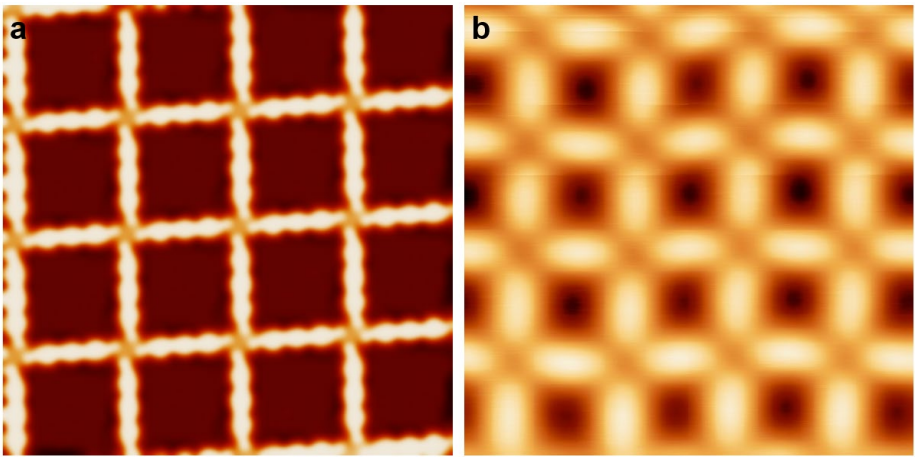

Figure S4. (a) Simulated STM image. (b) Experimental STM image. Scanning parameters: V_b = 500 mV and I_t = 100 pA, T = 4 K, image size: 8x nm^2.

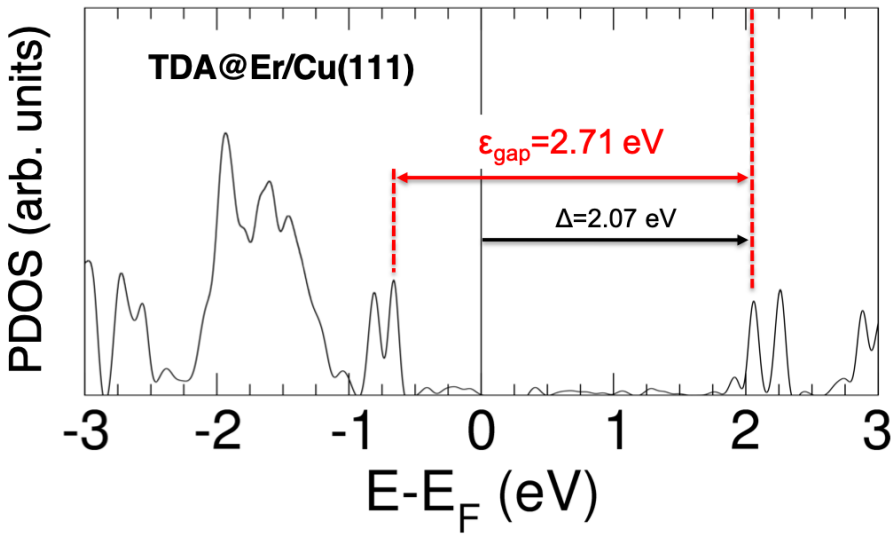

Figure S5. Computed density of states projected onto the TDA molecule for Er-coordinated TDA/Cu(111) interfaces.

Multiplet calculations

XAS, XMCD and XLD spectra were simulated using the MultiX code.[S18] MultiX uses a point charge model where the crystal field (CF) is simulated by the interaction of the magnetic atom with the charges of the surrounding atoms. DFT coordinates were used as a reference for the CF modelling. The CF was modelled considering the O and Cu atoms closest to the Er atom (see Figure S6). The O atoms were simulated with a -1.8 charge and the Cu with +0.05 based on the averaged values resulting from the DFT calculations. The Er^{3+} ion was simulated considering a $3d^{10}4f^{11}$ ground state, a temperature of 1.7 K, and magnetic fields of 0.05 for XLD and 6 T for XMCD and XLD. The Hartree-Fock parameters were rescaled by factors of 1.00 for the Coulomb interaction and 0.98 for the spin-orbit coupling, and a core-hole broadening of 0.60 eV was used to reproduce the experimental resolution and a scaling factor of 1.5 was applied to the CF.

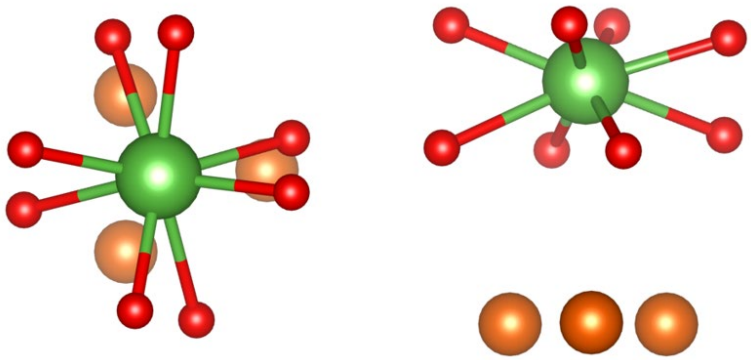

Figure S6. Front and side views of the crystal field used in the multiplet calculations. O, Er and Cu atoms are represented by red, green, and orange balls, respectively.

References

[S1] A. Barla, J. Nicolas, D. Cocco, S. M. Valvidares, J. Herrero-Martın, P. Gargiani, J. Moldes, C. Ruget, E. Pellegrin and S. Ferrer, *J. Synchrotron Rad*., 2016, **23**, 1507.

[S2] B. T. Thole, P. Carra, F. Sette and G. van der Laan, *Phys. Rev. Lett.*, 1992, **68**, 1943.

[S3] P. Carra, B. T. Thole and M. Altarelli, X. Wang, *Phys. Rev. Lett.*, 1993, **70**, 694.

[S4] Y. Teramura, A. Tanaka, B. T. Thole, and T. Jo, *J. Phys. Soc. Jpn.*, 1996, **65**, 3056.

[S5] I. Piquero-Zulaica, J. Lobo-Checa, A. Sadeghi, Z. M. Abd El-Fattah, C. Mitsui, T. Okamoto, R. Pawlak, T. Meier, A. Arnau, J. Enrique Ortega, J. Takeya, S. Goedecker, E. Meyer and S. Kawai, *Nat. Comm*., 2017, **8**, 787.

[S6] J. Lobo-Checa, M. Matena, K. Müller, J. H. Dil, F. Meier, L. H. Gade, T. A. Jung and M. Stöhr, *Science*, 2009, **325**, 300.

[S7] F. Forster, A. Bendounan and J. ZiroffF. Reinert, *Surf. Sci*., 2006, **600**, 3870.

[S8] I. Piquero-Zulaica, Z. M. Abd El-Fattah, O. Popova, S. Kawai, S. Nowakowska, M. Matena, M. Enache, M. Stöhr, A. Tejeda, A. Taleb, E. Meyer, J. E. Ortega, L. H. Gade, T. A. Jung and J. Lobo-Checa, *New J. Phys.*, 2019, **21**, 053004.

[S9] F. Klappenberger, D. Kühne, W. Krenner, I. Silanes, A. Arnau, F. J. García de Abajo, S. Klyatskaya, M. Ruben and J.V. Barth, *Phys. Rev. Lett.*, 2011, **106**, 026802.

[S10] I. Piquero-Zulaica, J. Li, Z. M. Abd El-Fattah, L. Solianyk, I. Gallardo, L. Monjas, A. K. H. Hirsch, A. Arnau, J. E. Ortega, M. Stöhr and J. Lobo-Checa, *Nanoscale*, 2019, **11**, 23132.

[S11] P. Giannozzi, S. Baroni, N. Bonini, M. Calandra, R. Car, C. Cavazzoni, D. Ceresoli, G. L. Chiarotti, M. Cococcioni, I. Dabo, A. Dal Corso, S. de Gironcoli, S. Fabris, G. Fratesi, R. Gebauer, U. Gerstmann, C. Gougoussis, A. Kokalj, M. Lazzeri, L. Martin-Samos, N. Marzari, F. Mauri, R. Mazzarello, S. Paolini, A. Pasquarello, L. Paulatto, C. Sbraccia, S. Scandolo, G. Sclauzero, A. P. Seitsonen, A. Smogunov, P. Umari, R. M. Wentzcovitch, *J. Phys.: Condens. Matter*., 2009, **21**, 395502.

[S12] L. A. Constantin, J. P. Perdew, J. M. Pitarke, *Phys. Rev. B*, 2009, **79**, 075126.

[S13] J. P. Perdew, A. Ruzsinszky, G. I. Csonka, O. A. Vydrov, G. E. Scuseria, L. A. Constantin, X. Zhou, K. Burke, *Phys. Rev. Lett*., 2008, **100**, 136406.

[S14] G. Kresse, J. Joubert, *Phys. Rev. B*, 1999, **59**, 1758.

[S15] J. D. Pack, H. J. Monkhorst, *Phys. Rev. B*, 1977, **16**, 1748.

[S16] S. Grimme, J. Antony, S. Ehrlich, H. Krieg, *J. Chem. Phys*., 2010, **132**, 154104.

[S17] M. Methfessel, A. T. Paxton, *Phys. Rev. B*, 1989, **40**, 3616.

[S18] A. Uldry, F. Vernay and B. Delley, *Phys. Rev. B*, 2012, **85**, 125133.

[S19] S. O. Parreiras, D. Moreno, B. Cirera, M. A. Valbuena, J. I. Urgel, M. Paradinas, M. Panighel, F. Ajejas, M. A. Niño, J. M. Gallego, M. Valvidares, P. Gargiani, W. Kuch, J. I. Martínez, A. Mugarza, J. Camarero, R. Miranda, P. Perna and D. Écija, *Small*, 2021, **17**, 2102753.